Adakite magmatism within the Sabzevar ophiolite zone, NE Iran: U-Pb geochronology and Sr-Nd isotopic evidences

Khadije Jamshidi[1*], Habibollah Ghasemi[1], Laicheng Miao[2], Mahmoud Sadeghian[1]

[1] *Department of Petrology, School of Geosciences, Shahrood University of Technology, Shahrood, P.O.Box 3619995161 Iran*

[2] *Institute of Geology and Geophysics, Chinese Academy of Sciences, Beijing, 100029, P.O. Box 9825 China*

*Corresponding author, e-mail: khj.jamshidi@yahoo.com

Abstract

Numerous post-ophiolite intrusions exposed into the late Cretaceous–Paleocene Sabzevar ophiolite belt, northeast Iran. The intrusions consist of calc-alkaline intermediate to felsic rocks with metaluminous to peraluminous in nature and adakitic affinities. Based on U-Th-Pb dating on separated zircons by SHRIMP   , the emplacement age of these rocks into the ophiolite zone is constrained to ~45 Ma. All intrusions show similar MORB –like initial Nd and Sr values of 0.512911 to 0512846 and 0.704758 to 0.703790, respectively, with positive εNd (45 Ma) values of +5.26 to +6.45 implying their cogenetic nature. These isotopic signatures combined with geochemical evidences are corresponding to parental adakitic magmas derived from wet partial melting of a garnet-amphibolite source from Sabzevar subducted oceanic lithosphere. After emplacement in the deep magma storage region (equal to 700-900 MPa), this magma evolved to intensify adakitic signatures via amphibole–dominated magma fractionation.

Keywords: *Geochronology, Sr–Nd Isotopes, Adakite, Sabzevar, Iran.*

Introduction

The Sabzevar ophiolite belt with ~200km long and~10km wide is a highly dismembered ophiolite complex located along the northern boundary of the central Iranian microcontinent. This belt as one of the internal Iranian group of ophiolites and colored mélanges is a part of Tethyan ophiolite (Shojaat *et al.,* 2003). Numerous intrusions with intermediate to felsic compositions outcropped in the Sabzevar ophiolite belt (Ghasemi *et al.,* 2010; Jamshidi *et al.,* 2015a; Jamshidi *et al.,* 2015b; Rossetti *et al.,* 2014; Shabanian *et al.,* 2012; Spies *et al.,* 1983; Yousefi *et al.,* 2016). The adakitic signatures of these intrusions and their relationship with partial melting of an oceanic slab and/or a mafic lower crust melts was approved (Ghasemi *et al.,* 2010; Jamshidi *et al.,* 2015a; Jamshidi *et al.,* 2015b; Rossetti *et al.,* 2014; Shabanian *et al.,* 2012). Jamshidi *et al.* (2015b) presented geochemical data on whole rocks and main mineral phases (amphiboles, plagioclases and clinopyroxenes) from numerous adakitic intrusive samples in Sabzevar belt. They named these intrusions as "Sabzevar post-ophiolite adakites" and divided them into two parts, northern and southern suites. The northern suites display SiO_2 contents of 55 to 64 wt.% with andesite, trachyandesite/trachydacite to dacite in composition. These suites have metaluminous to peraluminous affinity with high Al_2O_3 (14.2–19.1 wt. %), Na_2O (3.9-7 wt. %) and K_2O contents (0.6–2.9 wt. %).

High-K calc-alkaline and peraluminous samples of the southern suites contain higher silica contents than the northern suites (65 to 73.6 wt. % in SiO_2), ranging from dacite, rhyodacite to rhyolite in composition, with high Al_2O_3 contents (15 to 21 wt. %) and alkali contents (K_2O contents of 1.3 to 4.2 wt.% and Na_2O of 3.5 to 7.1 wt. %). Both the samples from northern and southern suites contain high concentrations of Sr (138-894.5 ppm) and low concentrations of Y (2.2–19 ppm) and Yb (0.4–2 ppm) contents similar to the range observed in typical adakites (Jamshidi *et al.,* 2015b). The results of amphibole thermobarometry tested by Jamshidi *et al.* (2015b), offer two distinct levels of major crystallization and thus magma storage regions (~750 and~350MPa) for these intrusive rocks. This suggestion was supported by the results from pyroxene– melt barometry (550 to 730 MPa) and plagioclase–melt barometry (130 to 468 MPa). Also, the main role of amphibole fractionation from very hydrous magmas at deep crustal levels in intensifying adakite-type affinities was confirmed (Jamshidi *et al.,* 2015a; Jamshidi *et al.,* 2015b). Geochemically, this adakite magmatism interpreted as partial melts derived from Sabzevar Neotethyan subducted oceanic slab underneath the southern edge of the eastern Alborz zone (Jamshidi *et al.,* 2015a). Rossetti *et al.* (2014) worked on similar low-Mg# adakitic intrusive rocks in the Soltanabad area (in the northeast of the Sabzevar ophiolite

zone) and achieved same geochemical results. Also, they reported U-Pb zircon and $^{40}Ar/^{39}Ar$ white mica and amphibole dating and constrained the Sabzevar magmatism to the late Paleocene (at ca. 58 Ma). By presenting a set of U-Pb geochronological and isotopic data on some adakitic intrusions in the southern part of Sabzevar ophiolite belt, Jamshidi *et al.* (2015a) considered an oceanic subducted slab-derived source for generating adakitic magmas in early Eocene time (ca. 48 Ma). Also, Moghadam *et al.* (2016) obtained a same age range (ca. 45–47 Ma) for similar adakitic rocks in Sabzevar region and stated a mantle source metasomatised by slab–derived melts in the back–arc setting contributed to the Eocene flare–up in Iran.

Here, following Jamshidi *et al.* (2015b) works, we present a new set of zircon U-Pb dating data obtained by SHRIMP II ion microprobe and also Sr–Nd isotopic ratios from diverse post-ophiolite adakite intrusions in a wider region from northern to southern parts of Sabzevar ophiolite belt. The analyzed samples were selected based on compositional and regional scattering. We attempt to clarify the petrogenesis, probable source composition and effective evolutional processes in generating adakite magmatism in the region during the Paleocene-Eocene. With this purpose, whenever is needed, we used the geochemical data and thermobarometry results which were presented completely in our previous article Jamshidi *et al.* (2015b).

Geological review
As for other segments of the Alpine–Himalayan belt, the late Mesozoic northward motion of the Arabian plate towards Eurasia is associated with the subduction of the Neotethyan ocean under the Central Iranian Plateau. This event was accompanied by formatting of some back-arc basins in the upper Eurasian plate, with small oceanic domains cutting across Central Iran (Nain–Baft, Sabzevar, Sistan seaways) in the mid to late Cretaceous.

Iranian ophiolites which linking the east European ophiolites to the west Asian ophiolites represented the remnants of the Neotethyan ocean and these oceanic basins lithospheres surround the Central Iran. The NW-SE–trending Sabzevar ophiolite belt as a part of the Tethyan oceanic lithosphere (Sabzevar ocean), exposed an area north of Sabzevar, NE Iran (Fig. 1 a). This ophiolite belt (ca. 100 to 78 Ma) originated from a Mid-Ocean

Ridge Basalt (MORB)- type mantle source metasomatized by fluids or melts from subducted sediments, implying a supra-subduction zone environment (Moghadam *et al.,* 2014). The ophiolitic mantle sequence contains ultramafic rocks (harzburgite, dunite, lherzolite and chromitite) and the crustal sequence include supra-subduction type volcanism as well as plutonic mass with minor pillow and massive lavas (Jafari *et al.,* 2013; Moghadam *et al.,* 2014; Shojaat *et al.,* 2003). Following ophiolite emplacement, post-ophiolite magmatic activities with adakitic affinities occurred in the Sabzevar belt (Ghasemi *et al.,* 2010; Jamshidi *et al.,* 2015a; Jamshidi *et al.,* 2015b; Rossetti *et al.,* 2014; Shabanian *et al.,* 2012; Yousefi *et al.,* 2016). These adakitic rocks outcropped as widespread intrusions into the ophiolite mantle sequences (especially in serpentinized-hurzburgite suites) as small stocks, domes and rarely as dykes (Fig. 1a, b, c and Fig. 2 a, b).

Post-ophiolite adakites were occured mostly within the northern and southern part of the ophiolite belt, with magmatism comprised intermediate to felsic unites in the northern part (Fig. 2 b-e) and more felsic rocks dominating the southern part (Fig. 2 a, f and g). Field evidences and geological characteristics of these adakitic intrusions were considered by Jamshidi *et al.* (2015b), in detail. In contrast to earlier works which considered a Late Miocene–Pliocene age for outcropping of these rocks at the Earth's surface (Jamshidi *et al.,* 2014), the recent geochronological data on similar suites in the Soltanabad region (Rossetti et al., 2014) and in the south Sabzevar (Jamshidi *et al.,* 2015a; Moghadam *et al.,* 2016) restricts the Sabzevar adakite magmatism from the late Paleocene (at ca. 58Ma) up to Mid Eocene (45 Ma).

Analytical techniques
U–Th-Pb zircon geochronology
Eight fresh rock samples were selected for U–Th-Pb Pb analyses, four of them from northern part and the rest from the southern part. Zircons were extracted from crushed samples weighted 5-10 kg using heavy liquids and a Frantz magnetic separator at the Laboratory of the Institute of Regional Geology and Mineral Resources of Hebei Province, China, and then were handpicked, mounted in epoxy resin and polished until the grain centers exposed.
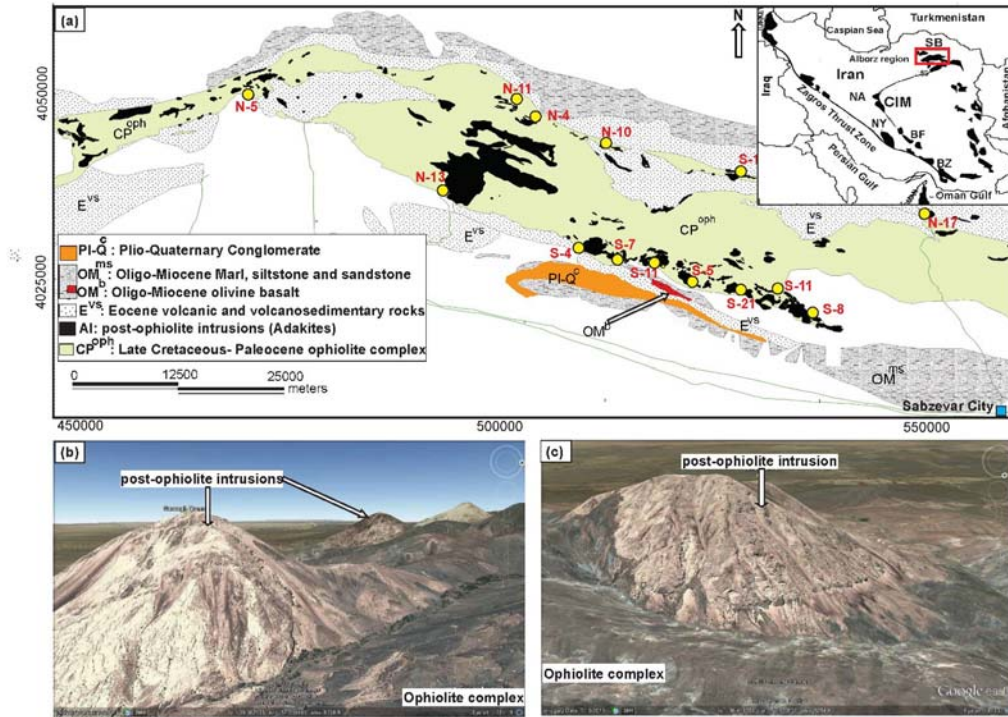
Figure 1. (a) Simplified geological map showing widespread distribution of post-ophiolite intrusions in the southern and northern parts of the Sabzevar ophiolite zone. Also, distribution of the main Iranian Mesozoic ophiolite belts (NA: Nain, NY: Neyriz, SB: Sabzevar, BF: Baft, BZ: Band-e-Ziyarat) is shown on the upright of the figure. Yellow circles display the locations of selected samples for separating zircons and isotopic analyses. (b) and (c) satellite images of post-ophiolite intrusions in the Sabzevar area.
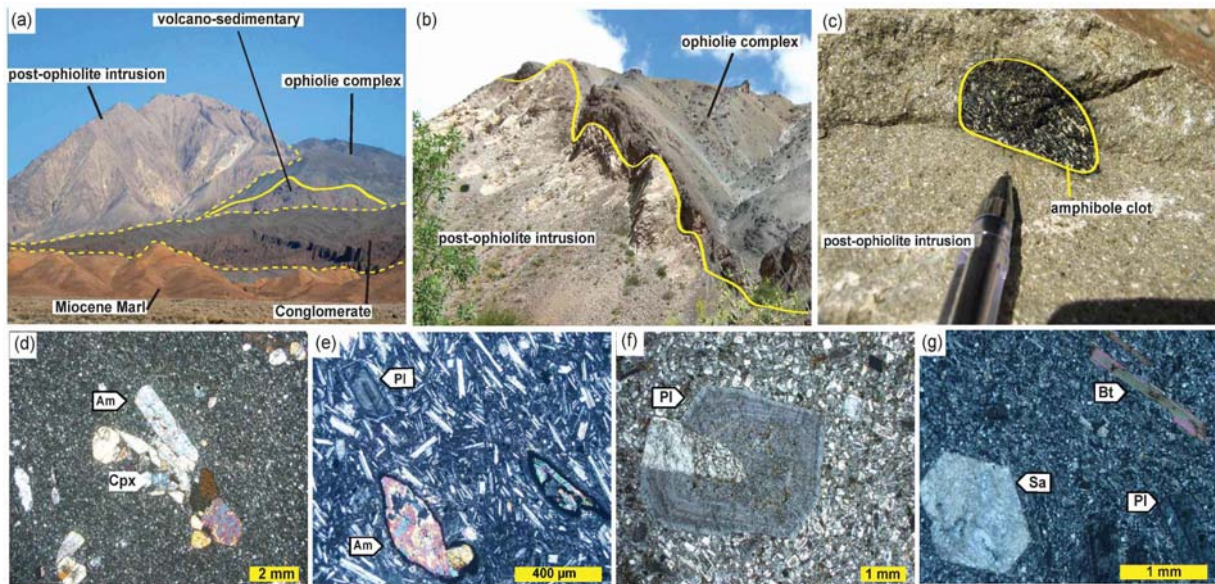

Figure 2. Field and microscopic (XPL) photographs. (a) Contact between post-ophiolite intrusions and host ophiolite-related harzburgite in the southern dome with rhyolite composition. Eocene volcanoclastic complex, Miocene sedimentary and Pliocene conglomerates are seen. (b) Northern grey dome of trachydacite exposed in ophiolite-related harzburgite and. (c) Presence of amphibole-dominated crystal clot in the northern trachyandesitic dyke. (d) Photomicrograph of amphibole and clinopyroxene phenocrysts in a fine-grain matrix in the Mg-andesite dyke. (e) Flow texture and presence of euhedral to subhedral amphiboles and plagioclases in andesite. (f) Zoned plagioclase phenocryst in dacite. (g) Altered sanidine, plagioclase and biotite in rhyolite. Mineral abbreviations include: Am —amphibole; Pl—plagioclase; Sa —Sanidine; Bt—biotite; Cpx— clinopyroxene, recommended by the IUGS: web version 01.02.07)

Before isotopic analysis, photographs under an optical microscope and cathodoluminescence (CL) images (Fig. 3) under a scanning electron microscopy (SEM) were respectively obtained in order to identify the morphology and internal textures and to choose potential target sites for later

U-Th-Pb analyses of the crystals. U-Th-Pb analyses on separated zircons were performed on the SHRIMP II ion microprobe at the Beijing SHRIMP Centre, Institute of Geology, Chinese Academy of Geological Sciences.
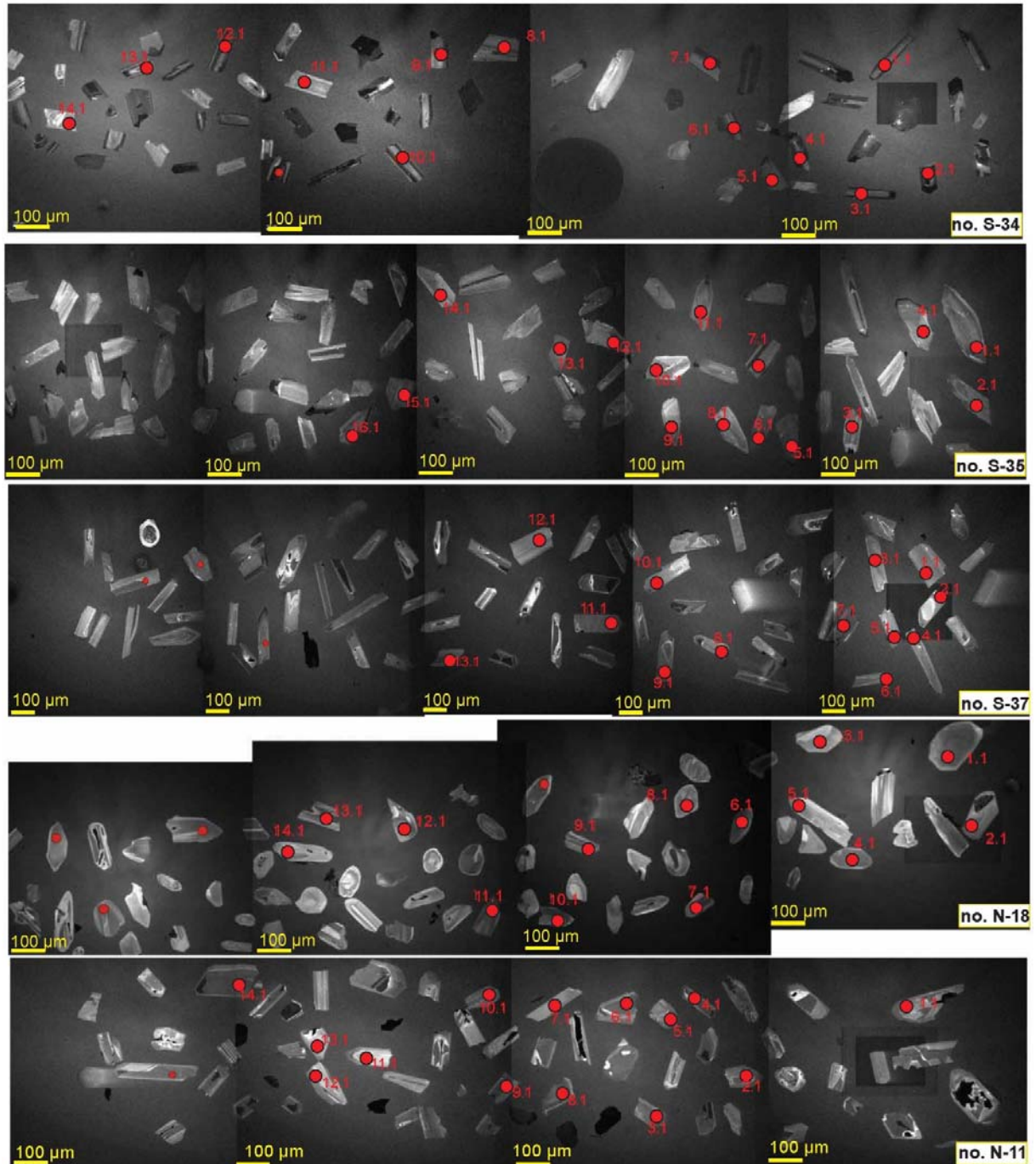

Figure 3 Cathodoluminescence (CL) images of zircon grains selected from a number of post-ophiolite adakitic samples. Targeted SHRIMP U–Pb analytical spots are indicated on the figures as solid circles.

The analytical procedures were similar to those described by Compston *et al.* (1992) and Compston *et al.* (1984). Mass resolution during the analytical sessions was ~5000 (1% definition), and the intensity of the primary ion beam was 5-8 nA. Primary beam size was normally 25-30 μm. Standards SL13 (U = 238 ppm) and TEMORA ($^{206}Pb/^{238}U$ age = 417 Ma) were used for calibrating the U abundance and isotope ratios, respectively. Decay constants used for age calculation are those recommended by Steiger & Jäger (1977). Measured ^{204}Pb was applied for the common lead correction and data processing was carried out using the SQUID and ISOPLOT programs (Ludwig, 2003). The uncertainties for individual analyses are quoted at the 1σ confidence level, whereas errors for pooled ages are quoted at 95% confidence. Due to small amount of ^{207}Pb formed in young (i.e. <1000 Ma) zircons, which results in low count rates and high analytical uncertainties, the determination of the ages for young zircons has to be primarily based on their $^{206}Pb/^{238}U$ ratios, whereas the older zircon ages are derived from $^{207}Pb/^{206}Pb$ ratios.

Sr and Nd isotopic analyses

The Rb–Sr and Sm–Nd isotopic analysis on thirteen whole-rock samples (six southern and seven northern samples) of Sabzevar post-ophiolite intrusions followed procedures similar to those described by (Li *et al.,* 2012b) and (Yang *et al.,* 2010). Whole rock powders for Sr and Nd isotopic analyses were dissolved in Savillex Teflon screw-top capsule after being spiked with the mixed ^{87}Rb–^{84}Sr and ^{149}Sm–^{150}Nd tracers prior to HF + HNO_3 + $HClO_4$ dissolution. Rb, Sr, Sm and Nd were separated using the classical two-step ion exchange chromatographic method and measured using a Thermo Fisher Scientific Triton Plus multi-collector thermal ionization mass spectrometer at Institute of Geology and Geophysics, Chinese Academy of Sciences (IGGCAS). The whole procedure blank was lower than 300pg for Rb-Sr and 100pg for Sm-Nd. The isotopic ratios were corrected for mass fractionation by normalizing to $^{88}Sr/^{86}Sr$=8.375209 and $^{146}Nd/^{144}Nd$ = 0.7219, respectively. The international standard samples, NBS-987 ($^{87}Sr/^{86}Sr$ =0.710250 ± 0.000021, n=9) and JNdi-1 ($^{143}Nd/^{144}Nd$ = 0.512118 ± 0.000014, n=9), were employed to evaluate instrument stability during the period of data collection. USGS reference material BCR-2 was measured to monitor the accuracy of the analytical procedures, with the following results: $^{87}Sr/^{86}Sr$ = 0.705028 ±0.000012 and $^{143}Nd/^{144}Nd$ = 0.512635 ±0.000014. The $^{87}Sr/^{86}Sr$ and $^{143}Nd/^{144}Nd$ data of BCR-2 show good agreement with previously published data by TIMS and MC-ICP-MS techniques (Li *et al.,* 2012a; Li *et al.,* 2012b).

Analytical results

Geochronology

Zircons are relatively scarce in the Sabzevar post-ophiolite intrusions. When present, zircon grains are mostly subhedral to euhedral, with elongated habits. They have oscillatory and planar magmatic growth zoning, usually with broadly homogeneous cores in CL images (Fig. 3). Most analyses represent high Th/U ratios (~0.42) which are characteristic of magmatic zircons (Wu & Zheng, 2004). Integrating crystal shapes, textures and Th/U contents for the majority of grains are presumed to be magmatic. U-Th-Pb analytical results of selected zircons from eight post-ophiolite samples are shown in Table 1. According to these results, all analyzed zircons represent the similar ranges of U-Pb age. They define concordant zircon $^{206}Pb/^{238}U$ ages ranging from 49.62 ± 0.76 (MSWD=0.92) to 42.98 ± 0.50 Ma (MSWD=1.3) (Fig. 4 and Fig. 5), which is interpreted as the crystallization age. All selected zircons combine to yield a mean age of 49.09 ±0.77 [1.6%] to 43.09 ± 0.59 Ma [1.4%] (2σ, conf. 95%) (Fig. 4 and Fig. 5), equivalent to the Early-Middle Eocene.

Nd and Sr isotopes

The results of Nd and Sr isotopic analyses on thirteen whole rocks are listed in Table 2. According to the U-Th-Pb geochronological results, the isotopic data were corrected for 45 Ma of radiogenic growth. The samples from various Sabzevar post-ophiolite intrusions are isotopically homogeneous and display initial $^{87}Sr/^{86}Sr$ and $^{143}Nd/^{143}Nd$ values of 0.704758 to 0.703790 and 0.512911 to 0512846 ,respectively, with positive εNd (45 Ma) values of +5.26 to +6.45, as same as these values in MORBs (Table 2). Both the northern and southern samples have similar Sr-Nd isotopic features, showing their origin from a same source.

Tectonic setting and genesis of Sabzevar post-ophiolite intrusions

Sabzevar post-ophiolite intrusions which are broadly distributed in the northern and southern parts of the Sabzevar ophiolite zone have intermediate to felsic compositions (Fig. 6 a).

Table 1. U-Th-Pb SHRIMP analytical data of zircons from Sabzevar post-ophiolite adakite samples.

Spot	U (ppm)	Th (ppm)	^{232}Th/^{238}U	^{207}Pb*/^{235}U	± (%)	^{207}Pb*/^{206}Pb	± (%)	^{206}Pb*/^{238}U	± (%)	^{206}Pb/^{238}U (Ma; ±1)
S-34-1.1	903	150	0.17	0.0493	4.6	0.0455	4.0	0.00786	2.2	50.7
S-34-2.1	1071	131	0.13	0.0494	4.0	0.0489	3.3	0.00733	2.2	46.7
S-34-3.1	1016	159	0.16	0.0493	4.8	0.0486	4.3	0.00735	2.2	47.1
S-34-4.1	886	138	0.16	0.0466	6.0	0.0458	5.6	0.00737	2.3	47.0
S-34-5.1	283	34	0.12	0.0500	10	0.0485	9.8	0.00749	2.7	47.1
S-34-6.1	409	29	0.07	0.0464	6.1	0.0422	5.6	0.00798	2.4	50.9
S-34-7.1	2300	2	0.00	0.0479	3.1	0.0466	2.4	0.00746	2.1	47.8
S-34-8.1	1241	934	0.78	0.0495	3.7	0.0482	3.0	0.00744	2.1	47.8
S-34-9.1	558	22	0.04	0.0468	5.4	0.0491	4.9	0.00691	2.3	44.3
S-34-10.1	535	40	0.08	0.0485	5.3	0.0490	4.6	0.00718	2.6	45.3
S-34-11.1	336	18	0.05	0.0421	7.2	0.0436	6.7	0.00701	2.5	44.1
S-34-12.1	738	124	0.17	0.0510	4.8	0.0510	3.9	0.00725	2.8	46.3
S-34-13.1	1111	1565	1.46	0.0596	3.3	0.0575	2.6	0.00751	2.1	47.6
S-35-1.1	1034	179	0.17	0.0480	4.3	0.0450	3.5	0.00776	2.5	49.7
S-35-2.1	867	165	0.19	0.0453	6.3	0.0420	5.7	0.00784	2.5	50.2
S-35-3.1	383	167	0.44	0.0430	13	0.0418	12	0.00757	2.7	48.0
S-35-4.1	795	138	0.17	0.0477	11	0.0462	11	0.00752	2.5	48.1
S-35-5.1	1134	189	0.17	0.0378	10	0.0371	9.9	0.00746	2.5	47.4
S-35-6.1	1137	189	0.17	0.0454	4.6	0.0440	3.9	0.00750	2.5	48.1
S-35-7.1	903	187	0.21	0.0395	13	0.0383	12	0.00755	2.5	48.0
S-35-8.1	527	208	0.39	0.0529	5.6	0.0496	5.0	0.00775	2.6	49.7
S-35-9.1	421	175	0.42	0.0734	13	0.0644	12	0.00801	3.2	50.1
S-35-10.1	737	335	0.45	0.0480	6.8	0.0469	6.3	0.00744	2.5	47.7
S-35-11.1	1007	198	0.20	0.0477	6.0	0.0465	5.4	0.00744	2.5	47.8
S-35-12.1	568	204	0.36	0.0470	5.6	0.0469	4.9	0.00728	2.6	46.6
S-35-13.1	935	153	0.16	0.0520	4.9	0.0491	4.2	0.00767	2.5	49.3
S-35-14.1	506	219	0.43	0.0401	12	0.0406	12	0.00726	2.6	46.0
S-35-15.1	818	141	0.17	0.0342	14	0.0340	14	0.00742	2.5	46.9
S-35-16.1	1175	182	0.16	0.0478	7.0	0.0470	6.5	0.00739	2.5	47.4
S-37-1.1	1951	89	0.05	0.0522	3.0	0.0487	2.3	0.00778	2.0	49.6
S-37-4.1	3154	77	0.03	0.0521	2.8	0.04772	2.0	0.00791	2.0	50.8
S-37-5.1	979	88	0.09	0.0534	3.7	0.0501	3.1	0.00773	2.1	48.7
S-37-6.1	3056	66	0.02	0.0505	2.7	0.04785	1.7	0.00766	2.0	49.2
S-37-7.1	2146	78	0.04	0.0505	3.0	0.0476	2.2	0.00769	2.0	49.2
S-37-8.1	1222	255	0.22	0.0550	3.5	0.0513	2.8	0.00778	2.1	50.0
S-37-9.1	1253	134	0.11	0.0479	3.8	0.0455	3.1	0.00764	2.1	48.6
S-37-10.1	2245	133	0.06	0.0524	3.0	0.0485	2.1	0.00784	2.0	50.4
S-37-11.1	1005	216	0.22	0.0511	4.2	0.0502	3.6	0.00738	2.2	47.1
S-37-12.1	2751	109	0.04	0.0528	2.9	0.04870	2.0	0.00786	2.0	50.1
S-37-13.1	1565	91	0.06	0.0519	3.4	0.0502	2.7	0.00751	2.1	47.9
S-37-14.1	982	144	0.15	0.0516	4.3	0.0506	3.7	0.00739	2.2	47.0
S-40-1.1	965	101	0.11	0.0433	4.8	0.0469	4.2	0.00670	2.3	43.24
S-40-2.1	894	108	0.13	0.0399	5.1	0.0420	4.7	0.00688	2.0	43.78
S-40-3.1	1126	102	0.09	0.0392	4.6	0.0437	4.2	0.00651	1.9	42.18
S-40-4.1	1061	108	0.11	0.0396	4.6	0.0452	4.2	0.00636	1.9	41.19
S-40-5.1	920	73	0.08	0.0414	4.9	0.0451	4.5	0.00665	2.0	42.87
S-40-6.1	852	84	0.10	0.0407	6.4	0.0433	6.1	0.00682	2.0	43.51
S-40-7.1	873	91	0.11	0.0404	5.6	0.0440	5.3	0.00666	2.0	43.66
S-40-8.1	1105	115	0.11	0.0381	5.3	0.0418	5.0	0.00661	1.9	42.88
S-40-9.1	733	91	0.13	0.0415	5.5	0.0452	5.1	0.00666	2.0	42.23
S-40-10.1	688	371	0.56	0.0405	6.3	0.0421	5.9	0.00697	2.1	43.9
S-40-11.1	1018	93	0.09	0.0411	6.0	0.0446	5.7	0.00669	2.0	43.24
S-40-12.1	973	82	0.09	0.0442	4.7	0.0471	4.3	0.00681	2.0	43.46
S-40-13.1	474	38	0.08	0.0440	7.0	0.0449	6.7	0.00711	2.2	45.9
S-40-14.1	957	80	0.09	0.0385	5.3	0.0419	4.7	0.00667	2.3	43.01

Table 1. Continued

| Spot	U (ppm)	Th (ppm)	$^{232}Th/^{238}U$	$^{207}Pb*/^{235}U$	± (%)	$^{207}Pb*/^{206}Pb$	± (%)	$^{206}Pb*/^{238}U$	± (%)	$^{206}Pb/^{238}U$ (Ma; ±1)
N-13-1.1	269	240	0.92	0.0389	11	0.0420	10	0.00671	2.5	43.4
N-13-2.1	190	135	0.74	0.0435	12	0.0438	12	0.00720	2.7	46.4
N-13-3.1	575	374	0.67	0.0543	5.7	0.0539	5.3	0.00730	2.2	46.5
N-13-4.1	326	219	0.69	0.0561	6.5	0.0551	6.1	0.00739	2.3	47.0
N-13-5.1	212	128	0.62	0.0557	9.1	0.0517	8.7	0.00780	2.5	49.8
N-13-6.1	415	304	0.76	0.0432	7.5	0.0439	7.2	0.00714	2.2	46.0
N-13-7.1	198	119	0.62	0.0389	13	0.0369	13	0.00763	2.6	49.6
N-13-8.1	512	276	0.56	0.0477	7.7	0.0500	7.3	0.00691	2.5	44.2
N-13-9.1	729	1100	1.56	0.0727	4.1	0.0769	2.8	0.00685	3.0	42.4
N-13-10.1	341	228	0.69	0.0462	7.2	0.0462	6.9	0.00726	2.3	46.7
N-13-11.1	657	480	0.76	0.0429	5.3	0.0482	4.8	0.00645	2.4	41.39
N-13-12.1	418	294	0.73	0.0462	6.7	0.0473	6.4	0.00708	2.2	45.48
N-13-13.1	250	214	0.89	0.0488	8.1	0.0506	7.7	0.00699	2.4	44.7
N-13-14.1	179	112	0.65	0.0459	11	0.0460	11	0.00724	2.9	46.5
N-17-1.1	310	267	0.89	0.0440	8.6	0.0459	8.3	0.00695	2.3	44.3
N-17-2.1	217	143	0.68	0.0477	9.7	0.0490	9.4	0.00706	2.5	45.1
N-17-3.1	364	266	0.75	0.0517	7.9	0.0521	7.6	0.00719	2.3	46.0
N-17-4.1	247	147	0.61	0.0480	8.4	0.0468	8.0	0.00745	2.5	46.5
N-17-5.1	454	284	0.65	0.0400	7.3	0.0422	6.8	0.00688	2.6	44.1
N-17-6.1	317	248	0.81	0.0534	8.3	0.0548	8.0	0.00707	2.4	44.7
N-17-7.1	416	241	0.60	0.0554	6.0	0.0572	5.6	0.00702	2.2	44.4
N-17-8.1	315	327	1.07	0.0501	7.6	0.0526	7.2	0.00692	2.4	44.0
N-17-9.1	351	229	0.67	0.0380	9.3	0.0400	9.0	0.00689	2.3	44.3
N-17-10.1	795	689	0.90	0.0424	5.4	0.0476	4.8	0.00647	2.4	41.0
N-17-11.1	702	472	0.69	0.0456	5.2	0.0489	4.8	0.00675	2.0	42.77
N-17-12.1	440	286	0.67	0.0468	8.3	0.0474	8.0	0.00715	2.2	45.6
N-17-13.1	233	112	0.49	0.0427	10	0.0414	10	0.00748	2.5	47.3
N-17-14.1	210	128	0.63	0.0378	12	0.0386	12	0.00711	2.8	45.3
N-17-15.1	251	157	0.64	0.0296	15	0.0285	15	0.00755	2.5	48.9
N-18-1.1	271	260	0.99	0.0540	6.3	0.0557	5.6	0.00704	2.8	44.4
N-18-2.1	236	207	0.91	0.0551	5.9	0.0573	5.2	0.00698	2.9	43.1
N-18-3.1	79	47	0.62	0.0340	16	0.0341	15	0.00723	3.2	47.3
N-18-4.1	145	150	1.07	0.0564	7.6	0.0542	7.0	0.00755	2.9	46.8
N-18-5.1	76	60	0.81	0.0774	9.5	0.0742	9.0	0.00756	3.3	47.1
N-18-6.1	114	77	0.70	0.0413	12	0.0424	11	0.00706	3.0	44.9
N-18-7.1	163	171	1.08	0.0600	6.7	0.0605	6.1	0.00719	2.8	44.4
N-18-8.1	111	61	0.56	0.0456	10	0.0464	10	0.00713	3.0	47.0
N-18-9.1	315	432	1.42	0.0640	4.9	0.0673	4.2	0.00690	2.6	42.6
N-18-10.1	348	263	0.78	0.0487	5.8	0.0520	5.2	0.00680	2.6	43.2
N-18-11.1	286	193	0.70	0.0468	6.3	0.0496	5.7	0.00686	2.6	42.9
N-18-12.1	227	254	1.15	0.0426	7.5	0.0457	7.0	0.00676	2.7	42.9
N-18-13.1	360	526	1.51	0.0595	4.7	0.0599	4.0	0.00720	2.6	44.7
N-18-14.1	50	25	0.51	0.0484	20	0.0518	19	0.00678	3.6	46.2
N-11-1.1	256	13	0.05	0.0332	18	0.0335	18	0.00719	2.9	46.2
N-11-2.1	366	62	0.18	0.0450	18	0.0465	18	0.00702	3.0	45.1
N-11-3.1	1776	9	0.01	0.0567	4.9	0.0547	4.3	0.00752	2.4	48.3
N-11-4.1	1164	6	0.00	0.0577	9.0	0.0558	8.6	0.00750	2.5	48.1
N-11-5.1	1136	245	0.22	0.0494	4.4	0.0478	3.7	0.00751	2.5	48.2
N-11-6.1	1253	1	0.00	0.0462	6.3	0.0460	5.8	0.00729	2.5	46.8
N-11-8.1	566	13	0.02	0.0403	20	0.0403	19	0.00726	2.7	46.6
N-11-9.1	1286	2	0.00	0.0474	5.7	0.0467	5.1	0.00737	2.5	47.3
N-11-10.1	479	31	0.07	0.0457	16	0.0422	16	0.00785	2.7	50.4
N-11-11.1	90	3	0.03	0.039	34	0.041	34	0.00695	3.8	44.6
N-11-12.1	143	40	0.29	0.027	43	0.029	43	0.00695	3.6	44.6
N-11-13.1	241	12	0.05	0.0284	22	0.0283	21	0.00728	3.0	46.7
N-11-14.1	1454	1	0.00	0.0425	6.2	0.0428	5.7	0.00721	2.4	46.3
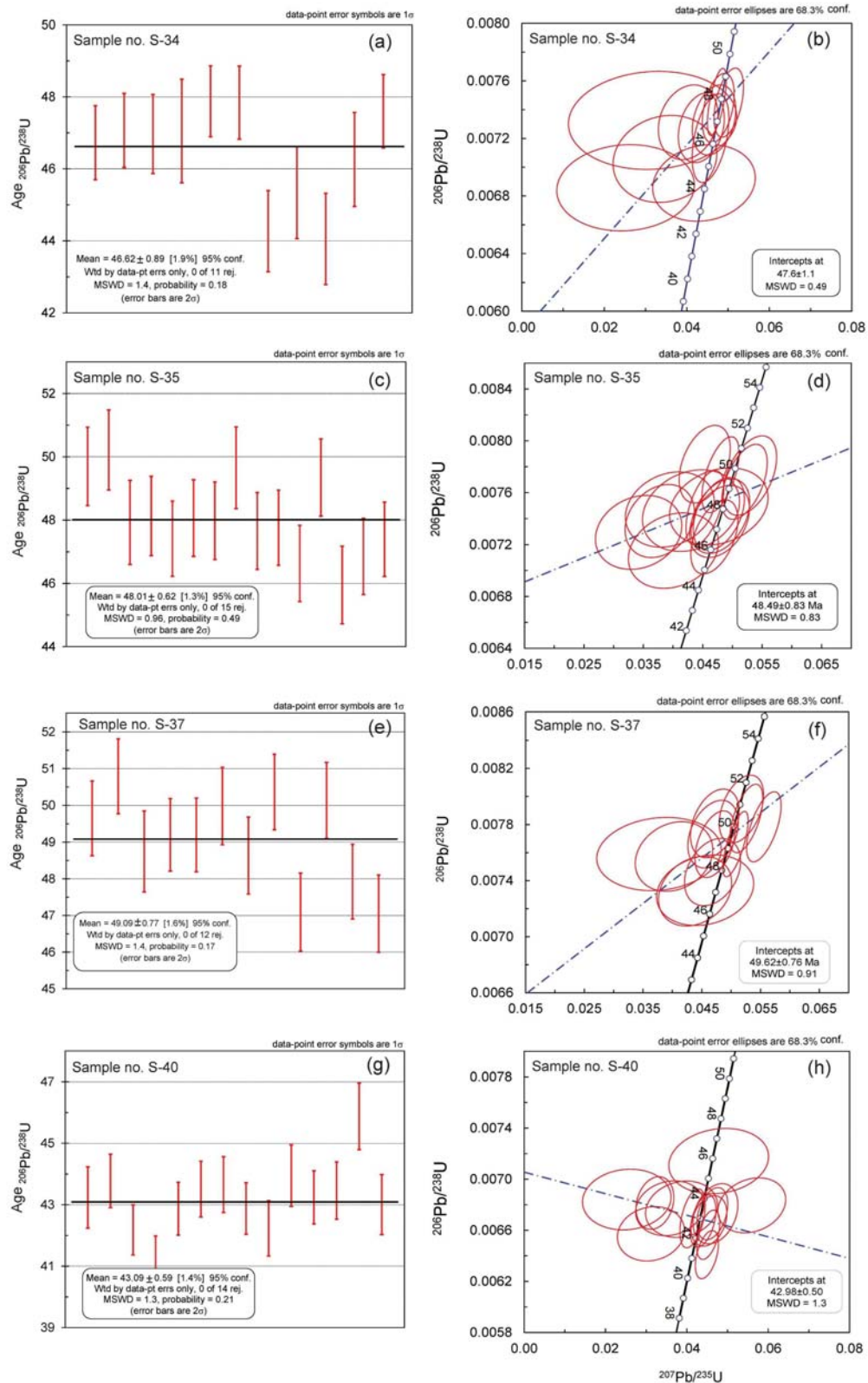
Figure 4. U–Pb concordia and mean age diagrams of zircons from Sabzevar post-ophiolite samples in the southern region.
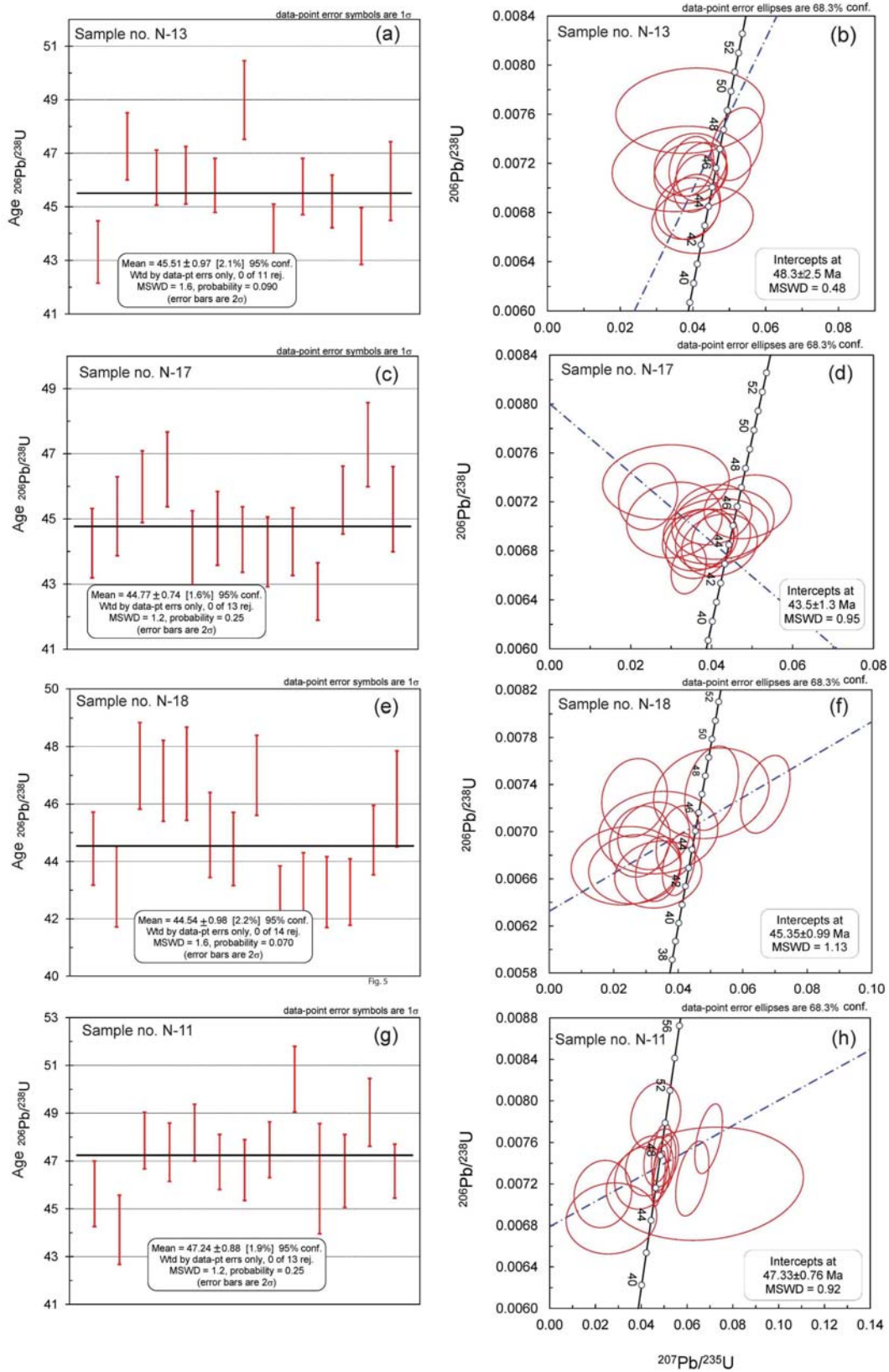
Figure 5. U–Pb concordia and mean age diagrams of zircons from Sabzevar post-ophiolite samples in the northern region.

Table 2. Nd and Sr isotopic data from thirteen samples of Sabzevar post-ophiolite intrusions.
Da: Dacite, Rhy: Rhyolite, T.da: trachydacite, An: Andesite

| Sample	Sm [ppm]	Nd [ppm]	$^{143}Nd/^{144}Nd$	I_{Nd} (45Ma)	εNd (45 Ma)	Error (2σ)	Rb [ppm]	Sr [ppm]	$^{87}Sr/^{86}Sr$	I_{Sr}	Error (2σ)
S-11(Da)	2.07	8.72	0.512944	0.512899	6.07	0.000009	25.95	284.25	0.70452	0.704341	0.000015
S-21(Da)	3.80	8.52	0.512930	0.512846	5.26	0.000008	23.15	668.57	0.70402	0.703954	0.000011
S-34 (Rhy)	0.91	4.08	0.512930	0.512888	6.09	0.000008	74.04	511.43	0.70437	0.704082	0.000012
S-35(Rhy)	1.02	4.81	0.512903	0.512863	5.59	0.000008	87.35	346.08	0.70429	0.703790	0.000011
S-37(Rhy)	0.70	3.95	0.512917	0.512883	5.99	0.000009	53.18	768.13	0.70456	0.704427	0.000014
S-40(Rhy)	1.84	9.64	0.512947	0.512911	6.52	0.000009	61.42	360.96	0.70414	0.703802	0.000013
N-4 (T.da)	2.14	8.37	0.51294	0.512892	6.15	0.000008	29.57	354.23	0.70444	0.704605	0.000015
N-5 (Da)	2.18	7.74	0.512942	0.512889	6.1	0.000010	14.23	61.30	0.70456	0.705019	0.000009
N- 10 (An)	2.81	12.78	0.512931	0.512889	6.11	0.000009	51.97	465.54	0.70390	0.704119	0.000009
N-11 (An)	2.67	12.24	0.512926	0.512885	6.03	0.000008	35.32	453.67	0.70394	0.704093	0.000012
N-13 (An)	8.97	52.97	0.512881	0.512849	5.32	0.000007	28.63	688.22	0.70418	0.704260	0.000015
N- 17 (An)	0.97	9.84	0.512882	0.512863	5.60	0.000008	10.46	416.17	0.70476	0.704808	0.000008
N-18 (Da)	2.51	13.46	0.512947	0.512911	6.54	0.000008	18.08	547.71	0.70385	0.703912	0.000015
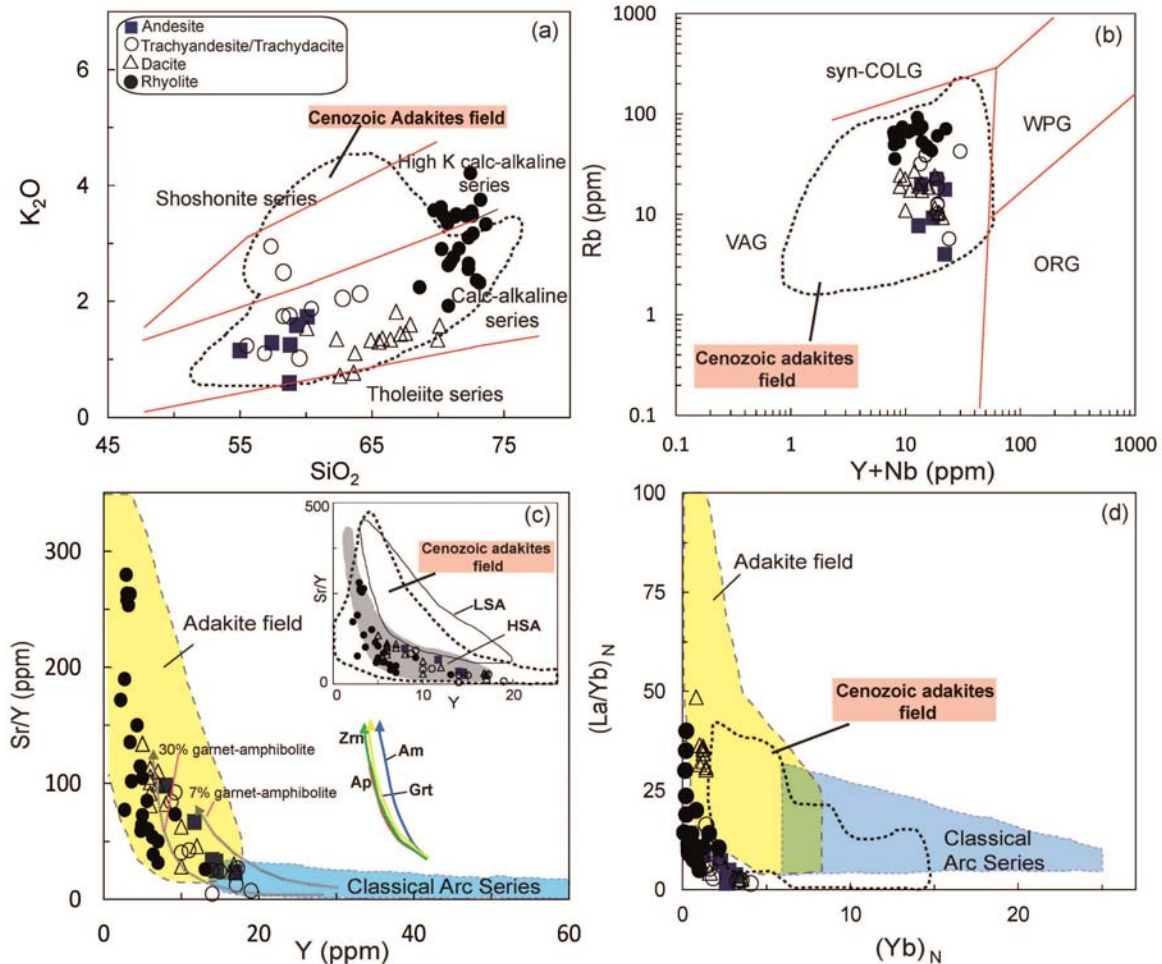
Figure 6. Selected major and trace element plots for post-ophiolite adakitic rocks. (a) K2O vs. silica diagram (after Peccerillo & Taylor, 1976), (b) Rb vs. Y+Nb tectonic discrimination diagram for granites (Pearce *et al.*, 1984). Sr/Y ratio vs. Y content (c) and (La/Yb)N vs. YbN (d), Fields of adakite and classical arc-series are from Defant & Drummond (1990) and Petford & Atherton (1996). Dotted fields correspond to Cenozoic adakite compositions after Lázaro & García-Casco (2008) and Lázaro *et al.* (2011, and refrencess there in). A Plot of Sr/Y vs. Y (c) after Martin *et al.* (2005) indicating the chemical differences between low silica adakites (solid field) and high-silica adakites (gray field). The discrimination lines are from Chen *et al.* (2016) using Rayleigh fractional crystallization models indicate the effects of garnet (Grt), amphibole (Am), zircon (Zrn) and apatite (Ap) fractionation on Sr/Y and Y.

As a geochemical review, these rocks indicate characteristic subduction-related trace-elements signatures, such as negative Nb, P and Ti anomalies combined with enriched LILE elements (Jamshidi *et al.,* 2015b). All intrusions represent subduction-related arc granitoids, belonging to calc-alkaline series (Fig. 6 a, b). Also, the samples mostly plot in the field of Cenozoic adakites (Fig. 6 a,b, c). Their adakitic signatures are implied from Sr (208-894.5) relative enrichment, Yb (0.05-2) and Y (2.2-19) depletion and negligible or absent Eu anomalies (Jamshidi *et al.,* 2015b). This is clearly appreciated in the Sr/Y versus Y diagram (Fig. 6 c) of Defant & Drummond (1990), where the intrusions plot in the adakite field although some felsic samples have very high Sr/Y values (>500) compared to typical adakites. In the $(La/Yb)_N$ vs. $(Yb)_N$ diagram (Fig. 6 d) of Defant & Drummond (1990), the felsic samples locate in the typical field of adakites although a number of intermediate samples plot outside this field as a result of their depletion in La. Totally, chemical characteristics of these intrusions allow them to be placed in adakite classification.

Before going through the possible origin/s of adakitic magma which, in our case, produced post-ophiolite intrusions, a brief review of the hypotheses related to adakitic magma generation is considered. Despite many works on adakite petrogenesis in recent decays, the resultant researches are full of arguments. Defant & Drummond (1990) proposed adakites are generated from direct melts of hot and young ($\leq$ 25 Ma) subducted oceanic slab. While many researchers showed that the adakitic rocks are not only the products of pristine subducted slab melts, but also they are generated by various petrogenetic processes in different tectonic setting (Atherton & Petford, 1993; Castillo, 2006; Castillo, 2012; Martin Martin *et al.,* 2005; Moyen, 2009; Xu *et al.,* 2002). The main purposed petrogenetic models are (1) Melting of the basaltic portion of the subducted oceanic lithosphere (Drummond & Defant, 1990) and subsequent variable interaction of slab-derived melts with the peridotitic mantle wedge (Martin *et al.,* 2005; Prouteau *et al.,* 2001; Rapp *et al.,* 1999; Stern & Kilian, 1996), (2) High-pressure fractionation of garnet and amphibole from a hydrous basaltic melt (Grove *et al.,* 2005; Macpherson *et al.,* 2006), (3) Partial melting of delaminated lower crust into the mantle (Xu *et al.,* 2002), which forms the melt with higher MgO and Ni and lower SiO_2, Al_2O_3 and Na_2O due to the

reaction with mantle, and (4) Partial melting of mafic continental lower crustal rocks (Atherton & Petford, 1993; Hou *et al.,* 2004; Wang *et al.,* 2006). Additionally, two main types of modern adakites are defined by Martin *et al.* (2005). One consists of high silica adakites (HSA) which represent subducted slab melts which have interacted with peridotite during their ascent through the mantle wedge. The second type consists of low silica adakites (LSA) which is considered to have generated by melting of a mantle wedge peridotite whose composition has been modified by reaction with felsic slab- melts.

Some samples of the southern region show higher K_2O contents (Fig. 6a) and peraluminous nature compared to ideal adakite magmatism. These may introduce the probable role of lower continental crust origin in generating adakitic magma in Sabzevar region. The data obtained in this research rule out this assumption, but instead, they highly favor an origin by melting of subducted slab. The possibility that melting of the subducted oceanic crust (Sabzevar Ocean, here) generated the Sabzevar post-ophiolite adakites during the early Cenozoic time discussed as follows.

Geochemical evidences to subducted-derived melt
Sabzevar post-ophiolite adakites put into the high silica adakites (HSA) field on Sr/Y versus Y diagram (Fig. 6 c). As mentioned before, HSA is interpreted as a result of partial melting of subducted basaltic slab at pressures high enough to stabilise garnet (eclogite or garnet-bearing amphibolite) (Martin *et al.,* 2005). Low amounts of MgO (avg. 1.7 wt.%) and Ni (up to 20 ppm) contents and high values of SiO_2 (> 60 wt.%), Al_2O_3 (14.2-20.6 wt.%), Na_2O (3.4-7.1 wt.%), lower $(Dy/Yb)_N$, and distinctive low K_2O/ Na_2O ratios (> 0.5) in the most samples of Sabzevar post-ophiolite adakites (Jamshidi *et al.,* 2015b) are sufficient to disprove the petrogenetic model in which lower-crustal delamination and then interaction with mantle coincided with adakite magmatism.

Furthermore, high contents of MgO and Ni in a few intermediate samples may be due to interaction between subducted slab-melt and mantle wedge peridotite during ascent which is considered as a significant factor in adakite magmatism events in many regions of the world (Bourdon *et al.,* 2002; Martin *et al.,* 2005; Rapp *et al.,* 1999; Zhu *et al.,* 2009) According to MgO and Ni vs. SiO_2 diagrams

(Fig. 7 a,b) of Wang *et al.* (2006), northern post ophiolite samples plot in the subducted slab–derived adakites. While the southern felsic ones with lower MgO and Ni contents put in the overlapping field of lower crustal- derived adakites and metabasaltic/ eclogitic melts (Fig. 7 a) and the field of lower crustal- derived adakites in the Fig. 7 b. Also, the distribution of samples on K_2O/Na_2O vs. Al_2O_3 diagram (Fig. 7 c) after Martin (1999) which is defined based on the typical Cenozoic adakites values ($K_2O/Na_2O \leq 0.5$, $Al_2O_3 \geq 15$ wt.%) is more consistent with our favorite generating model.

Trace elements signatures of Sabzevar post ophiolite adakites show more consistent with slab melting than magma originating from the lower crust (Fig. 7 d to h).
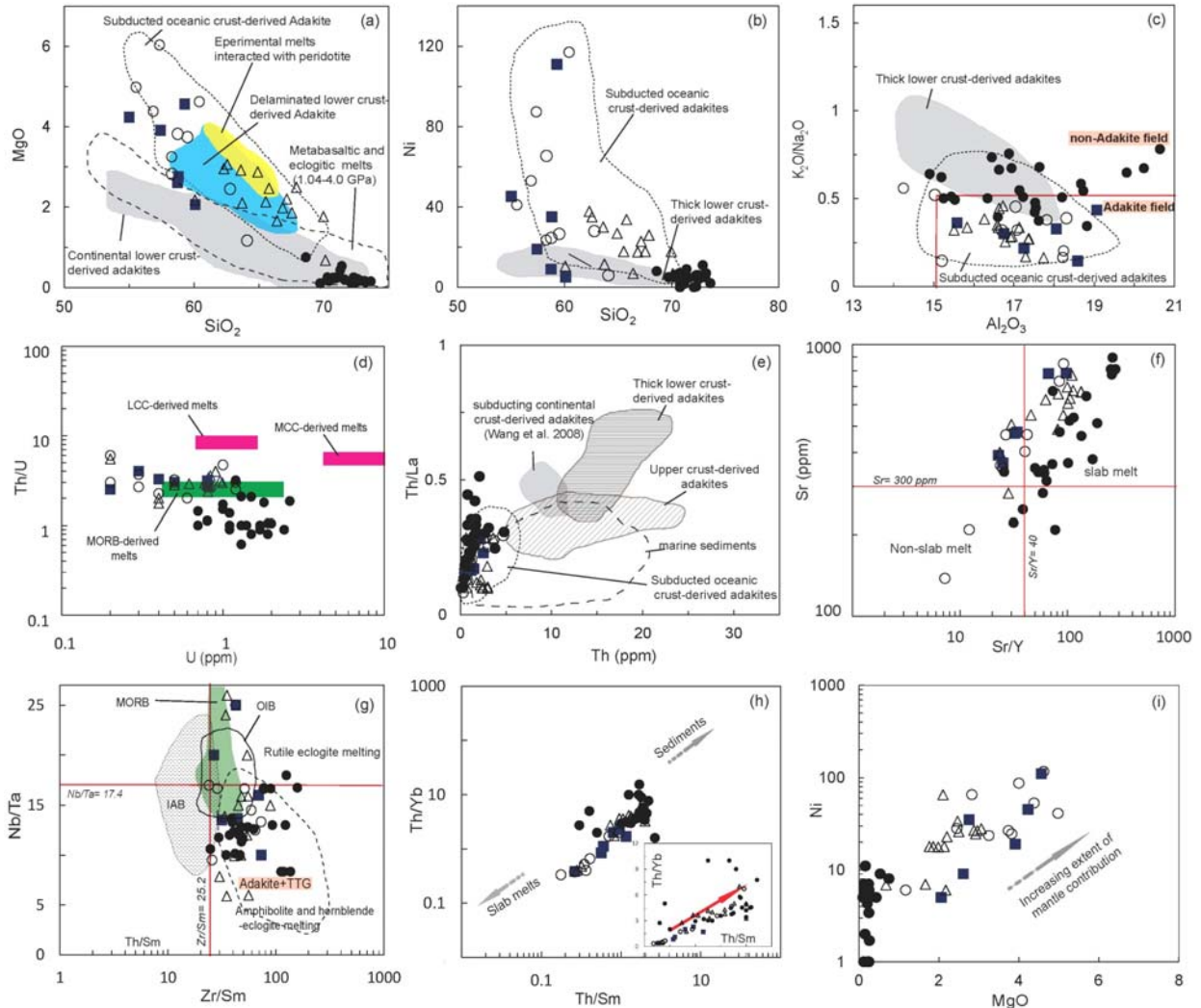
Figure 7. plots of main element oxides and trace elements for Sabzevar post-ophiolite intrusions (a) and (b) MgO and Ni vs. SiO_2 contents from Wang *et al.* (2006), (c) K_2O/Na_2O vs. Al_2O_3 content. The "adakite" and "non-adakite" fields are based on the amounts of K_2O/Na_2O (≤ 0.5) and Al_2O_3 (≥ 15 wt. %) in the Cenozoic adakites after Defant & Drummond (1990) and Martin (1999). The fields of subducted oceanic crust-derived adakites (Defant *et al.,* 1991; Kamei *et al.,* 2004) and the thick lower crust-derived adakites (Petford & Atherton, 1996; Topuz *et al.,* 2011) are shown on plot. (d) Th/U vs. U content, fields of LCC (lower continental crust) and MCC (middle continental crust) are from Rudnick & Gao (2003) and the field of MORB is after Sun *et al.* (2008). (e) Th content vs. Th/La ratio from Eyuboglu *et al.* (2012), (f) Sr/Y vs. Sr content, the "slab melt" and "non-slab melt" fields are based on classical adakite geochemistry after Whalen *et al.* (2002). (g) Nb/Ta vs Zr/Sm ratios (after Condie, 2005). Fields of MORB, OIB and IAB are after Foley *et al.* (2002) and the amounts Nb/Ta (17.4) and Zr/Sm (25.2) ratios are taken from Sun & McDonough (1989). (h) Th/Yb vs. Th/Sm from Zhu *et al.* (2009). Field of "slab melt" was described by Sun & McDonough (1989) and (i) Ni concentration vs. MgO after Pang *et al.* (2016).

The continental adakites tend to be K-rich and are distinguished by high contents of strongly incompatible elements such as Rb, Th and U (Wang *et al.,* 2008). Instead of a few samples from southern region,the Sabzevar post-ophiolite adakitic samples are Na-rich and have lower U (0.1-2.6 ppm), Th (0.1-4.8 ppm) contents and Th/U (0.1-6) ratios (see Jamshidi *et al.* 2015 a) than those of the lower crustal-derived adakites, but instead, their contents are similar to those of the Cenozoic slab-derived adakites in arc setting (Wang *et al.,* 2008). The Th/U values of both the northern and southern samples plot in approximity to the field of MORB – derived melts rather than in the area of lower or middle continental crustal (LCC, MCC) melts (Fig. 7 d). Also, formation of Sabzevar post-ophiolite adakites by melting of subducted oceanic crust indicated in the plots of Th vs. Th/La and Sr/Y vs. Sr contents (Fig. 7 e, f) after Whalen *et al.* (2002). Only few samples plot in the non-slab melt field (Fig. 7 f).

Remarkable geochemical evidences such as HREE, Y and HFSE (Nb, Ti) depletions, high Sr, Sr/Y and $(Gd/Yb)_N$ (>1) values with the absence of a negative Eu anomaly (See Jamshidi *et al.,* 2015b), suggest that the post-ophiolite adakitic magmas likely have been generated in upper pressure stability for plagioclase (> 1.6 GPa). These results combined with increasing trend of Sr/Y (Fig. 6c) and $(La/Yb)_N$ ratios (Fig. 6d) with differentiation can imply to garnet-amphibolite or eclogite source region for the Sabzevar adakites. The petrogenesis of typical adakitic magma is related to the presence of significant amounts of garnet ± amphibole either as a residual or an early crystallizing phase. An amphibolite source for Sabzevar adakites is supported by lower Nb/Ta ratio than primitive mantle value of 17.4 and the decrease of this Nb/Ta with increase in Zr/Sm ratios (Fig. 7g). The depletion of the HFSEs refers to amphibole as residual phase during melting of oceanic crust (Foley *et al.,* 2002; Klemme *et al.,* 2002). However, some intermediate samples contain lower La/Yb ratios than those in typical adakites (La/Yb> 16, Fig. 6d). This point to insignificant contribution of garnet to the melting reaction (Lázaro & García-Casco, 2008) in addition to this fact that LREE-bearing phase such as epidote and titanite were retained in the residual amphibolite (Lázaro & García-Casco, 2008; Rossetti *et al.,* 2014).

Compared to the typical subducted slab- derived adakites, some more evolved samples of southern

region are K-rich (K_2O up to 7wt%) and peraluminous (Jamshidi *et al.,* 2015b) and are apparently related to adakites of lower-crustal derivation. In contrast, a significant geochemical correlation between the southern high-silica and the northern intermediate adakites (Jamshidi *et al.,* 2015b) strengthen the hypothesis that the southern adakites are derived from the northern intermediate melts through continued magma chamber processes, e.g., fractional crystallization. Co-evolution of northern intermediate melts and southern felsic rocks is considered by Jamshidi *et al.* (2015b), in detail. Additionally,the peraluminous nature and high K values in some southern felsic rocks can be explained by contribution of subducted sediments during melting (Lázaro *et al.,* 2011). Present-day arc setting which significant amount of sediments are subducted typically show Th/Yb ratios >2, whereas arc setting without sediment contribution show Th/Yb ratios <1 (Nebel *et al.,* 2007; Woodhead *et al.,* 2001). Sabzevar adakites have Th/Yb ratios up to 10 (Jamshidi *et al.,* 2015b) suggesting a significant contribution of sediment in formation of parental magma. Linear trend of Sabzevar adakitic samples in a Th/Yb vs. Th/Sm (Fig. 7 h) from Zhu *et al.* (2009) supported this argument. This plot indicates that melting of subducted slab combined with a partial melt of subducted sediment formed adakitic magma in the region. Further, some intermediate samples have generally high MgO, Ni and Cr related to slab-derived adakites (Fig. 7i). This points to interaction with mantle peridotites, an inference to reconcile for for a model involving slab melts ascended through a mantle wedge (Pang *et al.,* 2016).

Isotopic evidences for subducted- related melt
Typical Adakites should have low $^{87}Sr/^{86}Sr$ and high $^{143}Nd/^{144}Nd$, reflecting those of geochemically depleted oceanic basalt, whereas lower crust-derived adakites should have higher $^{87}Sr/^{86}Sr$ and lower $^{143}Nd/^{144}Nd$ (Castillo, 2012). Our Sr-Nd isotopic results (Table 2) also support an oceanic subducted slab origin for Sabzevar post-ophiolite adakites ($[^{143}Nd/^{144}Nd]_i$= 0.512846 to 0.512911, $[^{87}Sr/^{86}Sr]_i$= 0.703790 to 0.704758 and εNd (45Ma)= 5.26 to 6.54) rather than the lower continental crust. This origin is clearly exhibited in two plots of $[^{87}Sr/^{86}Sr]_i$ vs. εNd (t) and $[^{87}Sr/^{86}Sr]$ vs. Rb (Fig. 8 a and b) from Drummond *et al.* (1996). In the Fig. 8 a, all Sabzevar post-ophiolite adakitic rocks plot within the depleted mantle

quadrant, a field occupied by adakites derived from Cenozoic subducted oceanic lithosphere, produced by Defant *et al.* (1992).
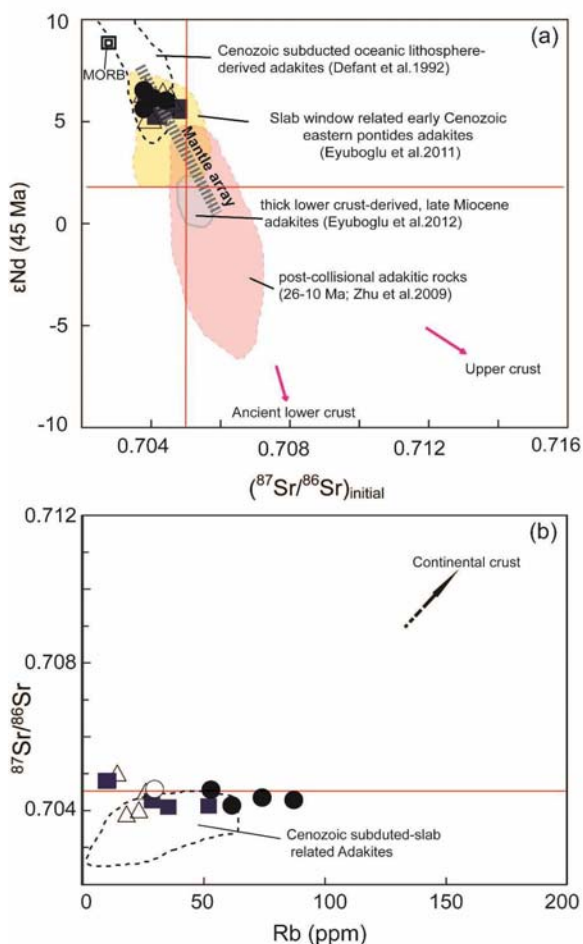

Figure 8. εNd (t= 45 Ma) vs. ^{87}Sr/^{86}Sr$_{initial}$ diagram (a) for post-ophiolite adakites from Sabzevar region. The fields of Cenozoic subducted oceanic lithosphere derived adakites (after Defant *et al.,* 1992), post-collisional adakites (after Zhu *et al.,* 2009) and thick lower crust-derived adakites (after Eyuboglu *et al.,* 2011) have been illustrated in the Diagram. ^{87}Sr/^{86}Sr vs. Rb diagram (b) from Drummond *et al.* (1996). Study rocks located in the Cenozoic subducted - slab related Adakites.

Role of amphibole-dominated fractionation

By describing many geochemical evidences such as the correlative variations in major- and trace- element ratios during magma differentiation, Jamshidi *et al.* (2015b) implied the co-evolution of northern intermediate and southern high-silica adakites in the Sabzevar region. Also, Sabzevar post- ophiolite intrusions show continuous trend with a more pronounced adakitic affinities that correlate with increasing differentiation in the Sr/Y vs. Y (Fig. 6c).These features combined with negative correlation of Al$_2$O$_3$, FeO$_t$, MgO, CaO, TiO$_2$, and trace elements

(Yb, V, and Y) with differentiation and lower MREE, (Tb=0.1 ppm) contents (Jamshidi *et al.,* 2015b) can be derived from amphibole-dominated fractionation during magma evolution. This is supported by remarkable increasing of Sr/Y (Fig. 6c), La/Yb (Fig. 6d), Zr/Sm (Fig. 7h) and Hf/Sm (Fig. 9 a) ratios and low Y and Yb concentrations in more evolved samples. Intense fractionation of amphibole increases the Sr/Y ratio and decreases the Y concentration and led the resulting melts to the strong adakitic affinities (Foley *et al.,* 2012). Also, amphibole crystallization will cause Hf/Sm increase in residual magmas (Fig. 9 a) because its high partition coefficient for Sm compared to Hf (Chen *et al.,* 2016). The plots of Ba vs. Rb and Rb/Sr vs. Sr/ Ba from Ding *et al.* (2011) display a trend consistent with fractional crystallization of amphibole during magma evolution (Fig, 8 b, c). Additionally, variating trends in the plots of Eu/Eu* vs. Sr content and (Dy/Yb)$_N$ vs. (La/Yb)$_N$ ratios (Fig. 9d,e) confirm a significant role of amphibole fractionation in combination with accessory minerals such as apatite and zircons to form adakite intrusions. Apatite fractionation can increase the Sr/Y ratio and Eu/Eu* (Fig. 9d), because

$$Kd_{Ap}^{Sm} = 46, \; K_{Ap}^{Eu} = 25.5 \text{ and } K_{Ap}^{Gd} = 43.9$$

(Fujimaki *et al.,* 1984). Also, zircon fractionation would increase (Dy/Yb)$_N$ and the La/Yb (Fig. 9e) and Sr/Y ratios of residue magmas (Chen *et al.,* 2016), because

$$Kd_{Zrn}^{Dy} = 0.140, \text{ and } Kd_{Zrc}^{La/Yb} = 0.005$$

(Bea *et al.,* 1994). The Nd (t) values and ^{87}Sr/^{86}Sr ratio of Sabzevar Adakites exhibit no obvious variation with increasing SiO$_2$ contents (Fig. 9 f, g) and Rb/Sr ratio (Fig. 9h), indicating that crustal assimilation did not play a significant role in their petrogenesis. This conclusion is consistent with fractional crystallization trend as a dominant factor in evolving magma which is illustrated in ^{87}Sr/^{86}Sr vs. MgO diagram (Fig. 9 i).

Geodynamic evolutions

As mentioned above, the subduction of the Neotethyan ocean under the central Iranian microcontinent has resulted in various styles of deformation and magmatism in different parts of the collision zone (Motaghi *et al.,* 2012; Shabanian *et al.,* 2012). The ongoing deformation is concentrated in the Zagros, Alborz and Kopeh Dagh Mountains, and in shear zones surrounding the Central Iranian microcontinent (Agard *et al.,* 2011; Motaghi *et al.,* 2012).
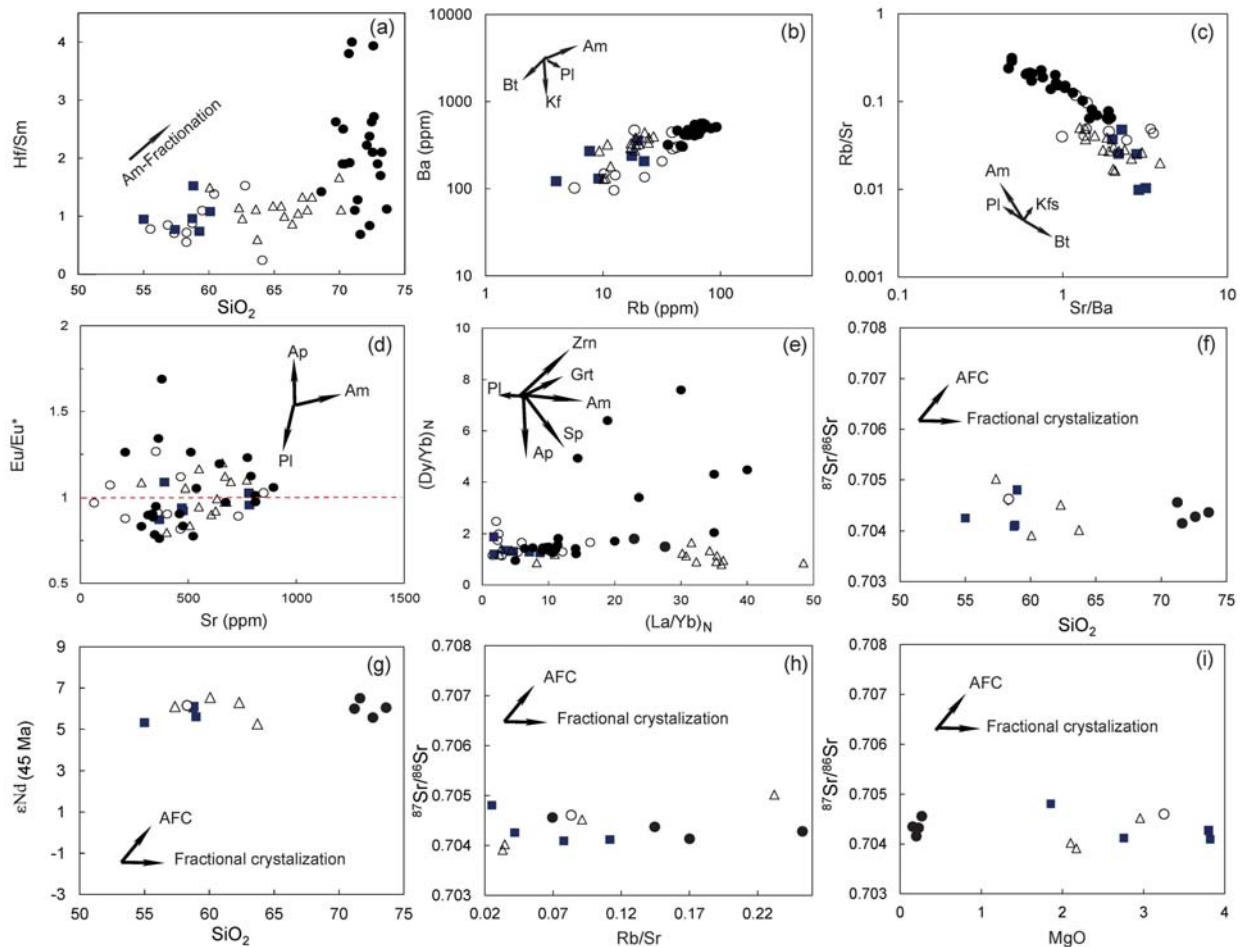
Figure 9. geochemical and isotopic plots for post-ophiolitic adakites: (a) Hf/Sm vs. SiO$_2$ content (after Chen *et al.,* 2016), (b) and (c) plots of Ba vs. Rb content and Rb/Sr vs. Sr/Ba ratios (after Ding *et al.,* 2011), (d) and (e) plots of Eu/Eu* vs. Sr content and (Dy/Yb)$_N$ vs. (La/Yb)$_N$ ratios from Chen *et al.* (2016). (f) and (g) SiO$_2$ content vs. $^{87}Sr/^{86}Sr$ ratios (after Varol *et al.,* 2007) and εNd (45 Ma) values (after Karsli *et al.,* 2011). (h) and (i) plots of Rb/Sr ratio vs. $^{87}Sr/^{86}Sr$ ratio and MgO content vs. $^{87}Sr/^{86}Sr$ ratios (after Varol *et al.,* 2007) geochemical diagrams for the studied. (Mineral abbreviations include: Am—amphibole; Pl—plagioclase; Grt— Garnet; Ap—Apatite; Sp— Sphene; Zrn—Zircon; Kfs— K-feldspars; Bt— biotite, recommended by the IUGS web version 01.02.07)

Accordong to Agard *et al.* (2011), this deformations can be summarized to: back-arc basin formation in the upper Eurasian plate with small oceanic domains cutting across Central Iran (Nain–Baft, Sabzevar, Sistan seaways) since Middle Jurassic (Ghasemi & Jamshidi, 2012, 2013) to Late Cretaceous, slab break-off along the Zagros orogen in late Paleocene, early Eocene compressional regimes with increasing collisional velocity, middle Eocene extentional regime overall upper plate espetially in Abbasabad- Sabzevar region (see also Ghasemi & Rezaei-Kahkhaei, 2015), late Eocene-early Oligocene compression, Oligo-Miocene extentional back- arc basin (Ghasemi & Barahmand, 2013; Ghasemi *et al.,* 2011; Ghasemi et *et al.,* 2016a; Ghasemi *et al.,* 2016b) and intensify

shortening from late Miocene (5-10 Ma) to present. It is widely believed that Sabzevar ocean as one of the several back-arc oceanic seaways in central Iran (e.g. Nain-Baft and Sistan seaway), opened during Cretaceous period and closed during the transition from Paleocene to Eocene (Agard *et al.*, 2011; Babazadeh & De-Wever, 2004; Omrani *et al.*, 2008; Rossetti *et al*., 2010; Shojaat *et al.*, 2003). Neo-Tethyan slab retreat, a process generally promoted in subduction zones by increased convergence velocities, is thought to have triggered the formation of these back-arc domains in this period (Agard *et al.,* 2011). Like other Iranian ophiolites, the Sabzevar ophiolite belt formed by obduction processes of this minor oceanic seaway, indicating discontinuous back-arc oceanic crust emplacement

(Agard *et al.,* 2011). Formation of Sabzevar ophiolite belt followed by long -lasting magmatic activities started since early Eocene and continued to the end of Pliocene (Ghasemi *et al.,* 2010; Shabanian *et al.,* 2012; Shojaat *et al.,* 2003; Spies *et al.,* 1983). Similar to the other region of the Alpine–Alpine–Himalayan belts (e.g. NE Turkey) and central Iran, the peak of subduction-related volcanism activities in the Sabzevar magmatic belt occurred in Eocene time. Our new geochronological data show an age range between 52 to 41 Ma (Early to Middle Eocene) for adakite magmatism event in the Sabzevar region. This time overlaps with the major pre-extensional arc magmatic phase in Central Iran presented by (Verdel *et al.,* 2011). This magmatism occurred in Paleocene-Early Eocene boundary and followed by Middle-Eocene extension with high volcanic output (Ghasemi & Rezaei-Kahkhaei, 2015) and latest Eocene - Early Oligocene, late- to post-extensional volcanism with back-arc basin geochemical affinity (Ghasemi & Barahmand, 2013; Ghasemi *et al.,* 2011; Ghasemi *et et al.,* 2016a; Ghasemi *et al.,* 2016b; Verdel *et al.,* 2011). According to our obtained ages (51-41 Ma) and geological context (specially intruding the adakites into the ophiolite sequence) and isotopic results, it can be deduced that partial melting of Sabzevar oceanic lithosphere which had controlled post-ophiolite volcanism in the Sabzevar region occurred at least at Late Paleocene or earliest Eocene. Water- saturated melting of a garnet-amphibolite source (Fig. 7h) during oceanic subduction could provide an appropriate condition for generating a magma with adakitic affinities. According to the thermobarometry results published (Jamshidi *et al.,* 2015b), Sabzevar post-ophiolite adakites record two distinct levels of magma storage. The amphibole in primitive samples (Mg-andesite) records mid- to lower crustal pressures ($\sim$700– 900MPa) that are in line with results from pyroxene– melt barometry. The other amphiboles show a shallower magma storage level equal to pressure of 300MPa, which is, in turn, supported by plagioclase–melt barometry results. The main role of amphibole fractionation in evolution of parental

high H_2O–magma was approved above. The event that let to intensifiy adakitic signatures of early deep slab-derived melts during their ascent to the shallower levels (upper crust). So that, the evolved phases (dacites and rhyolites) have more significant adakitic nature compared to the intermediate suites. This result consistent with some petrographic evidences such as the presence of amphibole and clinopyroxene phenocrysts with no plagioclase phenocryst in primitive andesite samples (Fig. 2d) and the existence of amphibole clots in intermediate rocks (Fig. 2c).

Conclusions

(i)Sabzevar Post-ophiolite intrusions with intermediate to felsic compositions crop out in diverse regions of Sabzevar ophiolite structural zone, especially in the southern and northern part. The zircon U–Pb dating of these intrusions yields the same age (45 Ma) all samples.

(ii) According to geochemical and MORB-like Sr-Nd isotopic data set presented here, all these calc-alkaline intrusions with adakitic signatures are co-genetic. The parental magma is best explained as resulting from the patial melting of Sabzevar subducted oceanic crust which has also experienced interaction with overlying lithospheric mantle during ascent.

(iii) Amphibole-dominated magma fractionation as a key process in intensifying adakite-type affinities occurred during magma ascent to the shallower levels. The event which in turn helped to generate the high silica adakite magmatism in the Sabzevar region during early to middle Eocene.

References

Agard, P., Omrani, J., Jolivet, L., Whitechurch, H., Vrielynck, B., Spakman, W., Monié, P., Meyer, B., Wortel, R., 2011. Zagros orogeny: a subduction-dominated process. Geological Magazine 148: 692-725.

Atherton, M.P., Petford, N., 1993. Generation of sodium-rich magmas from newly underplated basaltic crust. Nature 362: 144-146.

Babazadeh, S.A., De Wever, P., 2004. Early Cretaceous radiolarian assemblages from radiolarites in the Sistan Suture (eastern Iran). Geodiversitas 26: 185-206.

Bea, F., Pereira, M., Stroh, A., 1994. Mineral/leucosome trace-element partitioning in a peraluminous migmatite (a laser ablation-ICP-MS study). Chemical Geology 117: 291-312.

Bourdon, E., Eissen, J.-p., Monzier, M., Robin, C., Martin, H., Cotten, J., Hall, M.L., 2002. Adakite-like lavas from Antisana Volcano (Ecuador): evidence for slab melt metasomatism beneath Andean Northern Volcanic Zone. Journal of Petrology 43: 199-217.

Castillo, P.R., 2006. An overview of adakite petrogenesis. Chinese science bulletin 51: 257-268.

Castillo, P.R., 2012. Adakite petrogenesis. Lithos 134–135: 304-316.

Chen, S., Niu, Y., Li, J., Sun, W., Zhang, Y., Hu, Y., Shao, F., 2016. Syn-collisional adakitic granodiorites formed by fractional crystallization: Insights from their enclosed mafic magmatic enclaves (MMEs) in the Qumushan pluton, North Qilian Orogen at the northern margin of the Tibetan Plateau. Lithos 248: 455-468.

Compston, W., Williams, I., Kirschvink, J., Zichao, Z., Guogan, M., 1992. Zircon U-Pb ages for the Early Cambrian time-scale. Journal of the Geological Society 149: 171-184.

Compston, W., Williams, I., Meyer, C., 1984. U-Pb geochronology of zircons from lunar breccia 73217 using a sensitive high mass-resolution ion microprobe. Journal of Geophysical Research: Solid Earth 89.

Condie, K.C., 2005. TTGs and adakites: are they both slab melts? Lithos 80: 33-44.

Defant, M., Jackson, T., Drummond, M., De Boer, J., Bellon, H., Feigenson, M., Maury, R., Stewart, R., 1992. The geochemistry of young volcanism throughout western Panama and southeastern Costa Rica: an overview. Journal of the Geological Society 149: 569-579.

Defant, M.J., Drummond, M.S., 1990. Derivation of some modern arc magmas by melting of young subducted lithosphere. Nature 347: 662-665.

Defant, M.J., Richerson, P., De Boer, J.Z., Stewart, R.H., Maury, R.C., Bellon, H., Drummond, M.S., Feigenson, M.D., Jackson, T., 1991. Dacite genesis via both slab melting and differentiation: petrogenesis of La Yeguada volcanic complex, Panama. Journal of Petrology 32: 1101-1142.

Ding, L.-X., Ma, C.-Q., Li, J.-W., Robinson, P.T., Deng, X.-D., Zhang, C., Xu, W.-C., 2011. Timing and genesis of the adakitic and shoshonitic intrusions in the Laoniushan complex, southern margin of the North China Craton: implications for post-collisional magmatism associated with the Qinling Orogen. Lithos 126: 212-232.

Drummond, M., Defant, M., Kepezhinskas, P., 1996. Petrogenesis of slab-derived trondhjemite–tonalite-dacite/adakite magmas. Geological Society of America Special Papers 315: 205-215.

Drummond, M.S., Defant, M.J., 1990. A model for trondhjemite-tonalite-dacite genesis and crustal growth via slab melting: Archean to modern comparisons. Journal of Geophysical Research: Solid Earth 95: 21503-21521.

Eyuboglu, Y., Chung, S.-L., Santosh, M., Dudas, F.O., Akaryalı, E., 2011. Transition from shoshonitic to adakitic magmatism in the Eastern Pontides, NE Turkey: implications for slab window melting. Gondwana Research 19: 413-429.

Eyuboglu, Y., Santosh, M., Yi, K., Bektaş, O., Kwon, S., 2012. Discovery of Miocene adakitic dacite from the Eastern Pontides Belt (NE Turkey) and a revised geodynamic model for the late Cenozoic evolution of the Eastern Mediterranean region. Lithos 146: 218-232.

Foley, F.V., Pearson, N.J., Rushmer, T., Turner, S., Adam, J., 2012. Magmatic evolution and magma mixing of Quaternary adakites at Solander and little Solander Islands, New Zealand. Journal of Petrology, egs082.

Foley, S., Tiepolo, M., Vannucci, R., 2002. Growth of early continental crust controlled by melting of amphibolite in subduction zones. Nature 417: 837-840.

Fujimaki, H., Tatsumoto, M., Aoki, K.-I., 1984. Partition coefficients of Hf, Zr, and REE between phenocrysts and groundmasses, Lunar and Planetary Science Conference Proceedings, pp. B662-B672.

Ghasemi, H., Barahmand, M., 2013. Petrology and geochemistry of igneous rocks in the lower red formation, Garmsar area Quarterly Iranian Journal of Geology 7: 17-33.

Ghasemi, H., Barahmand, M., Sadeghian, M., 2011. The Oligocene basaltic lavas of east and southeast of Shahroud: Implication for back-arc basin setting of Central Iran Oligo-Miocene basin. Petrology (2228-5210), Scientific Quarterly Journal of University of Isfahan 2: 77-94.

Ghasemi, H., Jamshidi, K., 2012. Geochemistry, petrology and proposed tectonomagmatic model for generation of alkaline basic rocks in the base of the Shemshak Formation, the eastern Alborz zone. Iranian Journal of Crystallography and Mineralogy 19: 699-714.

Ghasemi, H., Jamshidi, K., 2013. Investigation of source region properties of alkaline basic rocks in the base of Shemshak Formation in the eastern Alborz zone. Quarterly Iranian Journal of Geology 7: 17-29.

Ghasemi, H., Rezaei-Kahkhaei, M., 2015. Petrochemistry and tectonic setting of the Davarzan-Abbasabad Eocene Volcanic (DAEV) rocks, NE Iran. Mineralogy and Petrology 109: 235-252.

Ghasemi, H., Rostami, M., Sadeghian, Kadkhodaye Arab, F., 2016a. Back-arc Extensional Magmatism in the Oligo-Miocene Basin of the Northern edge of Central Iran. . Geosciences, Scientific Quarterly Journal of Geological Survey of Iran 25: 239-252.

Ghasemi, H., Sadeghian, M., Khanalizadeh, A., Tanha, A., 2010. Petrography, geochemistry and radiometric ages of high-silica adakitic domes of Neogene continental arc, South of Quchan. Iranian J. Crystal. Mineral 3: 347-370.

Ghasemi, H., Sarizan, R., Taheri, A., 2016b. Source properties and tectonic setting of the basic magmatism in the Lower Red Formation, North of Garmsar (Semnan, Central Iran). . petrology (2228-5210), Scientific Quarterly Journal of University of Isfahan Acceptance for publishing.

Grove, T.L., Baker, M.B., Price, R.C., Parman, S.W., Elkins-Tanton, L.T., Chatterjee, N., Müntener, O., 2005. Magnesian andesite and dacite lavas from Mt. Shasta, northern California: products of fractional crystallization of H2O-rich mantle melts. Contributions to Mineralogy and Petrology 148: 542-565.

Hou, Z.-Q., Gao, Y.-F., Qu, X.-M., Rui, Z.-Y., Mo, X.-X., 2004. Origin of adakitic intrusives generated during mid-Miocene east–west extension in southern Tibet. Earth and Planetary Science Letters 220: 139-155.

Jafari, M.K., Babaie, H.A., Gani, M., 2013. Geochemical evidence for Late Cretaceous marginal arc-to-backarc transition in the Sabzevar ophiolitic extrusive sequence, northeast Iran. Journal of Asian Earth Sciences 70: 209-230.

Jamshidi, K., Ghasemi, H., Miao, L., 2015a. U-Pb age dating and determination of source region composition of post-ophiolite adakitic domes of Sabzevar Petrology (2228-5210) 6: 121-139.

Jamshidi, K., Ghasemi, H., Sadeghian, M., 2014. Petrology and geochemistry of the Sabzevar post-ophiolitic high silica adakitic rocks. Petrology (2228-5210) 5: 51–68.

Jamshidi, K., Ghasemi, H., Troll, V., Sadeghian, M., Dahren, B., 2015b. Magma storage and plumbing of adakite-type post-ophiolite intrusions in the Sabzevar ophiolitic zone, northeast Iran. Solid Earth 6: 1-24.

Kamei, A., Owada, M., Nagao, T., Shiraki, K., 2004. High-Mg diorites derived from sanukitic HMA magmas, Kyushu Island, southwest Japan arc: evidence from clinopyroxene and whole rock compositions. Lithos 75: 359-371.

Karsli, O., Ketenci, M., Uysal, İ., Dokuz, A., Aydin, F., Chen, B., Kandemir, R., Wijbrans, J., 2011. Adakite-like granitoid porphyries in the Eastern Pontides, NE Turkey: potential parental melts and geodynamic implications. Lithos 127: 354-372.

Klemme, S., Blundy, J.D., Wood, B.J., 2002. Experimental constraints on major and trace element partitioning during partial melting of eclogite. Geochimica et Cosmochimica Acta 66: 3109-3123.

Lázaro, C., Blanco-Quintero, I., Marchesi, C., Bosch, D., Rojas-Agramonte, Y., García-Casco, A., 2011. The imprint of subduction fluids on subducted MORB-derived melts (Sierra del Convento Mélange, Cuba). Lithos 126: 341-354.

Lázaro, C., García-Casco, A., 2008. Geochemical and Sr–Nd isotope signatures of pristine slab melts and their residues (Sierra del Convento mélange, eastern Cuba). Chemical Geology 255: 120-133.

Li, C.-F., Li, X.-H., Li, Q.-L., Guo, J.-H., Li, X.-H., Feng, L.-J., Chu, Z.-Y., 2012a. Simultaneous determination of 143Nd/144Nd and 147Sm/144Nd ratios and Sm–Nd contents from the same filament loaded with purified Sm–Nd aliquot from geological samples by isotope dilution thermal ionization mass spectrometry. Analytical chemistry 84: 6040-6047.

Li, C.-F., Li, X.-H., Li, Q.-L., Guo, J.-H., Li, X.-H., Yang, Y.-H., 2012b. Rapid and precise determination of Sr and Nd isotopic ratios in geological samples from the same filament loading by thermal ionization mass spectrometry employing a single-step separation scheme. Analytica chimica acta 727: 54-60.

Ludwig, K., 2003. User's manual for Isoplot 3.00: a geochronological toolkit for Microsoft Excel.

Macpherson, C.G., Dreher, S.T., Thirlwall, M.F., 2006. Adakites without slab melting: high pressure differentiation of island arc magma, Mindanao, the Philippines. Earth and Planetary Science Letters 243: 581-593.

Martin, H., 1999. Adakitic magmas: modern analogues of Archaean granitoids. Lithos 46: 411-429.

Martin, H., Smithies, R., Rapp, R., Moyen, J.-F., Champion, D., 2005. An overview of adakite, tonalite–trondhjemite–granodiorite (TTG), and sanukitoid: relationships and some implications for crustal evolution. Lithos 79: 1-24.

Moghadam, H.S., Corfu, F., Chiaradia, M., Stern, R.J., Ghorbani, G., 2014. Sabzevar Ophiolite, NE Iran: Progress from embryonic oceanic lithosphere into magmatic arc constrained by new isotopic and geochemical data. Lithos 210: 224-241.

Moghadam, H.S., Rossetti, F., Lucci, F., Chiaradia, M., Gerdes, A., Martinez, M.L., Ghorbani, G., Nasrabady, M., 2016. The calc-alkaline and adakitic volcanism of the Sabzevar structural zone (NE Iran): implications for the Eocene magmatic flare-up in Central Iran. Lithos 248: 517-535.

Motaghi, K., Tatar, M., Shomali, Z.H., Kaviani, A., Priestley, K., 2012. High resolution image of uppermost mantle beneath NE Iran continental collision zone. Physics of the Earth and Planetary Interiors 208: 38-49.

Moyen, J.F., 2009. High Sr/Y and La/Yb ratios: the meaning of the "adakitic signature". Lithos 112: 556-574.

Nebel, O., Münker, C., Nebel-Jacobsen, Y., Kleine, T., Mezger, K., Mortimer, N., 2007. Hf–Nd–Pb isotope evidence from Permian arc rocks for the long-term presence of the Indian–Pacific mantle boundary in the SW Pacific. Earth and Planetary Science Letters 254: 377-392.

Omrani, J., Agard, P., Whitechurch, H., Benoit, M., Prouteau, G., Jolivet, L., 2008. Arc-magmatism and subduction history beneath the Zagros Mountains, Iran: a new report of adakites and geodynamic consequences. Lithos 106: 380-398.

Pang, K.N., Chung, S.-L., Zarrinkoub, M.H., Li, X.-H., Lee, H.-Y., Lin, T.-H., Chiu, H.-Y., 2016. New age and geochemical constraints on the origin of Quaternary adakite-like lavas in the Arabia–Eurasia collision zone. Lithos 264: 348-359.

Pearce, J.A., Harris, N.B., Tindle, A.G., 1984. Trace element discrimination diagrams for the tectonic interpretation of granitic rocks. Journal of petrology 25: 956-983.

Peccerillo, A., Taylor, S.R., 1976. Geochemistry of Eocene calc-alkaline volcanic rocks from the Kastamonu area, northern Turkey. Contributions to mineralogy and petrology 58: 63-81.

Petford, N., Atherton, M., 1996. Na-rich partial melts from newly underplated basaltic crust: the Cordillera Blanca Batholith, Peru. Journal of Petrology 37: 1491-1521.

Prouteau, G., Scaillet, B., Pichavant, M., Maury, R., 2001. Evidence for mantle metasomatism by hydrous silicic melts derived from subducted oceanic crust. Nature 410: 197-200.

Rapp, R., Shimizu, N., Norman, M., Applegate, G., 1999. Reaction between slab-derived melts and peridotite in the mantle wedge: experimental constraints at 3.8 GPa. Chemical Geology 160: 335-356.

Rossetti, F., Nasrabady, M., Theye, T., Gerdes, A., Monié, P., Lucci, F., Vignaroli, G., 2014. Adakite differentiation and emplacement in a subduction channel: The late Paleocene Sabzevar magmatism (NE Iran). Geological Society of America Bulletin 126: 317-343.

Rossetti, F., Nasrabady, M., Vignaroli, G., Theye, T., Gerdes, A., Razavi, M.H., Vaziri, H.M., 2010. Early Cretaceous migmatitic mafic granulites from the Sabzevar range (NE Iran): implications for the closure of the Mesozoic peri-Tethyan oceans in central Iran. Terra Nova 22: 26-34.

Rudnick, R., Gao, S., 2003. Composition of the continental crust. Treatise on geochemistry 3: 1-64.

Shabanian, E., Acocella, V., Gioncada, A., Ghasemi, H., Bellier, O., 2012. Structural control on volcanism in intraplate post collisional settings: Late Cenozoic to Quaternary examples of Iran and Eastern Turkey. Tectonics 31, doi:10.1029/2011TC003042.

Shojaat, B., Hassanipak, A., Mobasher, K., Ghazi, A., 2003. Petrology, geochemistry and tectonics of the Sabzevar ophiolite, North Central Iran. Journal of Asian Earth Sciences 21: 1053-1067.

Spies, O., Lensch, G., Mihm, A., 1983. Geochemistry of the postophiolitic Tertiary volcanics between Sabzevar and Quchan (NE Iran). Rep Geol Miner Surv Iran 51: 247-266.

Steiger, R.H., Jäger, E., 1977. Subcommission on geochronology: convention on the use of decay constants in geo-and cosmochronology. Earth and planetary science letters 36: 359-362.

Stern, C.R., Kilian, R., 1996. Role of the subducted slab, mantle wedge and continental crust in the generation of adakites from the Andean Austral Volcanic Zone. Contributions to mineralogy and petrology 123: 263-281.

Sun, S.-S., McDonough, W.-s., 1989. Chemical and isotopic systematics of oceanic basalts: implications for mantle composition and processes. Geological Society, London, Special Publications 42: 313-345.

Sun, W., Hu, Y., Kamenetsky, V.S., Eggins, S.M., Chen, M., Arculus, R.J., 2008. Constancy of Nb/U in the mantle revisited. Geochimica et Cosmochimica Acta 72: 3542-3549.

Topuz, G., Okay, A.I., Altherr, R., Schwarz, W.H., Siebel, W., Zack, T., Satır, M., Şen, C., 2011. Post-collisional adakite-like magmatism in the Ağvanis Massif and implications for the evolution of the Eocene magmatism in the Eastern Pontides (NE Turkey). Lithos 125: 131-150.

Varol, E., Temel, A., Gourgaud, A., Bellon, H., 2007. Early Miocene adakite-like volcanism in the Balkuyumcu region, central Anatolia, Turkey: Petrology and geochemistry. Journal of Asian Earth Sciences 30: 613-628.

Verdel, C., Wernicke, B.P., Hassanzadeh, J., Guest, B., 2011. A Paleogene extensional arc flare-up in Iran. Tectonics 30.

Wang, Q., Wyman, D.A., Xu, J.-F., Zhao, Z.-H., Jian, P., Xiong, X.-L., Bao, Z.-W., Li, C.-F., Bai, Z.-H., 2006. Petrogenesis of Cretaceous adakitic and shoshonitic igneous rocks in the Luzong area, Anhui Province (eastern China): implications for geodynamics and Cu–Au mineralization. Lithos 89: 424-446.

Wang, Q., Wyman, D.A., Xu, J., Wan, Y., Li, C., Zi, F., Jiang, Z., Qiu, H., Chu, Z., Zhao, Z., 2008. Triassic Nb-enriched basalts, magnesian andesites, and adakites of the Qiangtang terrane (Central Tibet): evidence for metasomatism by slab-derived melts in the mantle wedge. Contributions to Mineralogy and Petrology 155: 473-490.

Whalen, J.B., Percival, J.A., McNICOLL, V.J., Longstaffe, F.J., 2002. A mainly crustal origin for tonalitic granitoid rocks, Superior Province, Canada: implications for late Archean tectonomagmatic processes. Journal of Petrology 43: 1551-1570.

Woodhead, J., Hergt, J., Davidson, J., Eggins, S., 2001. Hafnium isotope evidence for 'conservative'element mobility during subduction zone processes. Earth and Planetary Science Letters 192: 331-346.

Wu, Y., Zheng, Y., 2004. Genesis of zircon and its constraints on interpretation of U-Pb age. Chinese Science Bulletin 49: 1554-1569.

Xu, J.-F., Shinjo, R., Defant, M.J., Wang, Q., Rapp, R.P., 2002. Origin of Mesozoic adakitic intrusive rocks in the Ningzhen area of east China: Partial melting of delaminated lower continental crust? Geology 30: 1111-1114.

Yang, Y.-h., Zhang, H.-f., Chu, Z.-y., Xie, L.-w., Wu, F.-y., 2010. Combined chemical separation of Lu, Hf, Rb, Sr, Sm

and Nd from a single rock digest and precise and accurate isotope determinations of Lu–Hf, Rb–Sr and Sm–Nd isotope systems using Multi-Collector ICP-MS and TIMS. International Journal of Mass Spectrometry 290: 120-126.

Yousefi, F., Sadeghian, M., Samiari, S., Ghasemi, H., 2016. Geochemistry and tectonic setting of high silica adakititic domes of Ahmad Abad Khartouran (Southeast Shahrood). GEOSCIENCES, Scientific Quarterly Journal of Geological Survey of Iran 25: 239-252.

Zhu, D.-C., Zhao, Z.-D., Pan, G.-T., Lee, H.-Y., Kang, Z.-Q., Liao, Z.-L., Wang, L.-Q., Li, G.-M., Dong, G.-C., Liu, B., 2009. Early cretaceous subduction-related adakite-like rocks of the Gangdese Belt, southern Tibet: Products of slab melting and subsequent melt–peridotite interaction? Journal of Asian Earth Sciences 34: 298-309.